

A SCALABLE DEEP LEARNING APPROACH FOR SOLVING HIGH-DIMENSIONAL DYNAMIC OPTIMAL TRANSPORT*

WEI WAN[†], YUEJIN ZHANG[‡], CHENGLONG BAO[§], BIN DONG[¶], AND ZUOQIANG SHI[§]

Abstract. The dynamic formulation of optimal transport has attracted growing interests in scientific computing and machine learning, and its computation requires to solve a PDE-constrained optimization problem. The classical Eulerian discretization based approaches suffer from the curse of dimensionality, which arises from the approximation of high-dimensional velocity field. In this work, we propose a deep learning based method to solve the dynamic optimal transport in high dimensional space. Our method contains three main ingredients: a carefully designed representation of the velocity field, the discretization of the PDE constraint along the characteristics, and the computation of high dimensional integral by Monte Carlo method in each time step. Specifically, in the representation of the velocity field, we apply the classical nodal basis function in time and the deep neural networks in space domain with the H^1 -norm regularization. This technique promotes the regularity of the velocity field in both time and space such that the discretization along the characteristic remains to be stable during the training process. Extensive numerical examples have been conducted to test the proposed method. Compared to other solvers of optimal transport, our method could give more accurate results in high dimensional cases and has very good scalability with respect to dimension. Finally, we extend our method to more complicated cases such as crowd motion problem.

Key words. optimal transport, deep neural network, Lagrangian discretization, crowd motion, back propagation, adjoint state method

AMS subject classifications. 65K10, 68T05, 68T07

1. Introduction. Optimal transport (OT) [43, 52] is an exciting research topic that connects many subjects in mathematics including differential geometry, partial differential equations, optimization, probability theory. Since OT naturally presents a tool to study probability distributions, it has been applied to many tasks in machine learning [51], such as transfer learning [10, 40], generative models [5, 42, 28], image processing [35] and natural language processing [26]. Despite its numerical success, computing high-dimensional OT remains a challenge. Many traditional mesh-based discretization methods [36, 54, 30] suffer from the curse of dimensionality. The computation bottleneck limits the applications of OT for various high-dimensional problems, which motivates this work.

The OT problem is originated from Monge [33] that studies good transportation with minimal cost. Mathematically, let \mathcal{X} and \mathcal{Y} be two complete and separable metric spaces, $\mu \in \mathcal{P}(\mathcal{X})$ and $\nu \in \mathcal{P}(\mathcal{Y})$ are two probability measures, the **Monge**

*submitted to the editors April, 2022.

Funding: Chenglong Bao is supported by National Key R&D Program of China (No. 2021YFA1001300), National Natural Science Foundation of China (Grant No. 11901338), Tsinghua University Initiative Scientific Research Program. Bin Dong are supported in part by National Natural Science Foundation of China (Grant No. 12090022) and Beijing Natural Science Foundation (No. 180001). Zuoqiang Shi is supported by National Natural Science Foundation of China (Grant No. 12071244).

[†]School of mathematics and physics, North China Electric Power University.

[‡]Department of Mathematical Science, Tsinghua University.

[§]Yau Mathematical Sciences Center, Tsinghua University, and Yaqi Lake Beijing Institute of Mathematical Sciences and Applications.

[¶]Beijing International Center for Mathematical Research, Peking University, and Center for Machine Learning Research, Peking University.

problem is to find a transportation map $T : \mathcal{X} \rightarrow \mathcal{Y}$ such that it minimizes

$$(1.1) \quad \inf_T \left\{ \int_{\mathcal{X}} c(x, T(x)) d\mu(x) : T_{\#}\mu = \nu \right\},$$

where $c : \mathcal{X} \times \mathcal{Y} \rightarrow \mathbb{R}$ is the cost function and $T_{\#}$ is the push forward operator induced by T , i.e. $\nu(B) = \mu(T^{-1}(B))$ for all measurable set $B \subset \mathcal{Y}$. Directly solving (1.1) is a challenging problem as the (1.1) is highly nonconvex and the minimum does not exist in general.

One special choice of the cost function is the quadratic case, i.e. $c(x, y) = \|x - y\|^2$. The seminal work [8] proves that the optimal map T is the gradient of a convex function that satisfies the Monge-Ampère equation. The Monge-Ampère equation is a fully nonlinear PDE and its numerical solver is highly non-trivial. Many numerical methods have been developed based on this approach [7, 38, 29]. However, these methods discretize the computational domain by regular grids which is unaffordable for high dimensional problem. In [22], the variational principle of the OT problem is established by linking OT with power diagram in computational geometry. The resulted variational problem can be solved by convex optimization algorithm with applications to image generation [28, 3, 4].

Instead of finding a transport map, **Kantorovich formulation** [24] relaxes the Monge problem (1.1) by introducing a joint distribution $\gamma \in \Pi(\mu, \nu)$. The coupling set $\Pi(\mu, \nu)$ is defined as

$$\Pi(\mu, \nu) = \{\gamma \in \mathcal{P}(\mathcal{X} \times \mathcal{Y}) : (\pi_x)_{\#}\gamma = \mu, (\pi_y)_{\#}\gamma = \nu\},$$

where π_x and π_y are the two projections of $\mathcal{X} \times \mathcal{Y}$ onto \mathcal{X} and \mathcal{Y} , respectively. In this case, the Kantorovich formulation is to find γ by solving

$$(1.2) \quad \inf_{\gamma} \left\{ \int_{\mathcal{X} \times \mathcal{Y}} c(x, y) d\gamma(x, y) : \gamma \in \Pi(\mu, \nu) \right\}.$$

It is noted that when μ, ν are absolutely continuous with respect to the Lebesgue measure, the Kantorovich problem (1.2) has a unique solution [52, 53] of the form $\pi = (\text{Id} \times T)_{\#}\mu$, where Id stands for the identity map, and T is the unique minimizer of (1.1).

When μ and ν are discrete distributions, the Kantorovich problem (1.2) can be formulated as a standard linear program (LP) that can be solved by classical algorithms, e.g. simplex method. These methods have relatively high computational cost and do not fully exploited the structure in the Kantorovich formulation (1.2). The Sinkhorn method [11] introduced the entropy regularization into (1.2), that can be efficiently solved by the Sinkhorn algorithm [47]. Sinkhorn method significantly accelerates the computation of OT especially with GPU implementation. As dimension grows, the number of grid points in Sinkhorn method need to increase exponentially to achieve satisfactory accuracy which leads to high computational cost and memory requirement. For continuous cases, Genevay et al. [18] first proposed a stochastic gradient descent to optimize the regularized OT problem by expressing the dual variables in reproducing kernel Hilbert spaces (RKHS). Seguy et al. [45] proposed to use deep neural networks to parameterize the dual variables for computing an OT plan and then estimate an optimal map as a neural network learned by approximating the barycentric projection of the obtained OT plan. In addition, they theoretically prove the convergence of regularized OT plan. In recent papers, Makkuva et al. [32]

proposed a minimax optimization to learn the optimal Kantorovich potential. The key idea is to restrict the search over all convex functions with introducing a regularization constraint and approximate the optimal potential by an input convex neural networks (ICNN) [2].

The dynamic OT, an alternative formulation of OT, is first proposed in [6] that is to solve a PDE-constrained optimal control problem. Since the dynamic OT provides a close relationship with fluid mechanics, it has been extended to many applications including unnormalized OT [17], mean field games [27]. Borrowing the theory from continuum mechanics, there are many possibilities for developing OT problems under task-specific constraints, which makes the numerical solver for dynamic OT more attractive. In [6], it applies an Eulerian discretization and solve the constrained minimization problem with the augmented Lagrangian method. The staggered grid discretization is used in [36] that proposed a proximal splitting scheme. Based on [36], a primal-dual formulation of dynamic OT [23] is proposed under the Helmholtz-Hodge decomposition, which enforces the divergence-free constraints during iterations. Recently, Yu et al. [54] proposed an accelerated proximal gradient algorithm using multilevel and multigrid strategies to solve dynamic mean field planning problems, which can be viewed as a generalization of OT. Above methods can obtain good result in low-dimension cases, but cannot be readily extended to high dimensions.

In recent years, deep learning [44, 21] have demonstrated remarkable success on a variety of computational problems ranging from image classification [25, 49], speech recognition [1, 12] and natural language processing [9, 20], to numerical approximations of partial differential equations (PDEs) [14, 15, 48, 39]. Such numerical results suggest that deep neural networks have powerful approximation ability for high-dimensional functions (see [46, 31, 13] for the approximation theory). Based on the link between continuous normalizing flows and dynamic OT, the TrajectoryNet was proposed in [50] and applied for learning cellular dynamics. The network in [50] consists of three fully connected layers with leaky ReLU activations, and the loss function is carefully designed by imposing multiple biological priors. The regularized neural ordinary differential equation (RNODE) is proposed in [16] by penalizing the Frobenius norm of the Jacobian of the velocity field, which improves the training stability. The Frobenius norm and the divergence of the velocity field is calculated by Monte Carlo trace estimator. Very recently, Ruthotto et al. [41] proposed a machine learning based method for solving high-dimensional mean field game and mean field control problems (known as MFGnet). In their work, a neural network is proposed to represent the Kantorovich potential whose gradient is the velocity field and the Hamilton-Jacobi-Bellman (HJB) equation is employed as a regularization. Numerically, it needs to compute the second derivative of the potential model and the number of training samples and the running time per iteration have noticeable growth as the dimension increases.

In this work, we propose a new deep learning approach for solving the high-dimensional dynamic OT. We adopt the Lagrangian discretization to solve the continuity equation and use Monte Carlo sampling to approximate the integrals in high dimensions rather than mesh-based discretization. Moreover we carefully designed a neural network for parametrizing the velocity field. Our approach only needs to calculate the first derivative of the neural network with respect to the input. In summary, the contributions of this paper are as follow.

- We present a novel approach to parameterize the velocity field by combining neural network in space and linear finite element basis in time. Based on the priori information that the characteristics of the optimal solution are straight,

we introduce the Frobenius norm of the Jacobian of the velocity field as the regularization to improve generalization.

- Our proposed framework is easy to implement and can be extended to more complicated problem, such as crowd motion. The proposed algorithm has much lower computational cost while the accuracy is comparable with state-of-the-art methods, Sinkhorn and MFGnet, especially for high-dimensional cases.

The rest of our paper is organized as follows. In Section 2, we introduce the dynamic OT problem, the proposed model parameterized by a neural network, and the back propagation method for solving the dynamic OT problems. Experimental results and some details about implementation are summarized in Section 3. Finally, we conclude this work in Section 4.

2. The Proposed Framework to Solve Dynamic OT.

2.1. Preliminaries on Dynamic OT. In this paper, we mainly consider the dynamic OT problem introduced by Benamou and Brenier [6]. The basic problem can be formulated as follows: Given two probability densities ρ_0 and ρ_1 , we want to find the density $\rho : \mathbb{R}^d \times [0, 1] \rightarrow \mathbb{R}$ and the velocity field $\mathbf{v} : \mathbb{R}^d \times [0, 1] \rightarrow \mathbb{R}^d$ that transport the mass of ρ_0 to the mass of ρ_1 at minimal transport cost $\mathcal{E}(\rho, \mathbf{v})$, i.e.,

$$(2.1) \quad \min_{(\rho, \mathbf{v}) \in \mathcal{C}(\rho_0, \rho_1)} \mathcal{E}(\rho, \mathbf{v}) := \int_0^1 \int_{\Omega} |\mathbf{v}(x, t)|^2 \rho(x, t) dx dt$$

and any pair of $(\rho, \mathbf{v}) \in \mathcal{C}(\rho_0, \rho_1)$ satisfies continuity equation with initial and terminal densities of ρ being ρ_0, ρ_1 provided as:

$$(2.2) \quad \mathcal{C}(\rho_0, \rho_1) := \{(\rho, \mathbf{v}) : \partial_t \rho + \nabla \cdot (\rho \mathbf{v}) = 0, \rho(\cdot, 0) = \rho_0, \rho(\cdot, 1) = \rho_1\}.$$

Note that in the whole paper, ∇ and $\nabla \cdot$ denote the gradient and the divergence w.r.t. the space variable x , respectively. In addition, the relationship of the optimal map T and the optimal solution (ρ, \mathbf{v}) is that:

$$(2.3) \quad \rho(\cdot, t) = (T_t)_\# \rho_0 \text{ with } T_t(x) = (1 - t)x + tT(x),$$

$$(2.4) \quad v_t = \left(\frac{d}{dt} T_t \right) \circ T_t^{-1} = (T - \text{id}) \circ T_t^{-1}.$$

Note that $\mathcal{E}(\rho, \mathbf{v})$ denotes the generalized kinetic energy and the optimal $\mathcal{E}(\rho, \mathbf{v})$ gives the square of the L^2 Wasserstein distance. This fluid mechanics formulation provides a natural time interpolation which is very useful in many applications.

2.2. Relaxation of Dynamic OT. First, we relax the constraint on the terminal density into an implicit condition by introducing a Kullback–Leibler (KL) divergence penalty term:

$$\mathcal{P}(\rho) := \lambda \int_{\Omega} \rho(x, 1) \log \frac{\rho(x, 1)}{\rho_1(x)} dx.$$

Note that $\mathcal{P}(\rho)$ is the KL divergence between $\rho(\cdot, 1)$ and ρ_1 up to a sufficiently large positive constant λ , which is the penalty parameter.

From (2.3) we know that the characteristic of the optimal solution T_t is a straight line connecting the source point x and the target point $T(x)$. However, the integrated kinetic energy $\mathcal{E}(\rho, \mathbf{v})$ forces the dynamics to travel in straight lines only on

the training data. In order to improve generalization during training and enhance the smoothness of the velocity field, we introduce the Frobenius norm of the Jacobian of the velocity field as the regularization $\mathcal{R}(\mathbf{v})$, i.e.,

$$\mathcal{R}(\mathbf{v}) := \alpha \int_0^1 \int_{\Omega} |\nabla \mathbf{v}(x, t)|_F^2 dx dt,$$

where $|\cdot|_F$ denotes Frobenius norm and α is a positive regularization parameter.

By relaxing the terminal density as an implicit condition penalized by KL divergence term $\mathcal{P}(\rho)$ and introducing the regularization term $\mathcal{R}(\mathbf{v})$, we can get the following optimal control formulation:

$$(2.5) \quad \min_{(\rho, \mathbf{v}) \in \mathcal{C}(\rho_0)} \mathcal{F}(\rho, \mathbf{v}) = \mathcal{E}(\rho, \mathbf{v}) + \mathcal{P}(\rho) + \mathcal{R}(\mathbf{v}),$$

where $\mathcal{C}(\rho_0) := \{(\rho, \mathbf{v}) : \partial_t \rho + \nabla \cdot (\rho \mathbf{v}) = 0, \rho(\cdot, 0) = \rho_0\}$.

2.3. Lagrangian Discretization. In order to solve the high-dimensional OT problems, we naturally adopt the Lagrangian discretization method instead of the traditional mesh-based method. Because the Lagrangian discretization is a sampling method that can reduce memory usage by overcoming the spatial discretization into grids. Firstly, the continuity equation in $\mathcal{C}(\rho_0)$ can be solved along the characteristics:

$$(2.6) \quad \frac{d}{dt} \mathbf{z}(x, t) = \mathbf{v}(\mathbf{z}(x, t), t), \mathbf{z}(x, 0) = x,$$

$$(2.7) \quad \frac{d}{dt} \rho(\mathbf{z}(x, t), t) = -\rho(\mathbf{z}(x, t), t) \nabla \cdot \mathbf{v}(\mathbf{z}(x, t), t), \rho(\mathbf{z}(x, 0), 0) = \rho_0(x).$$

Note that the equation (2.7) is equivalent to

$$(2.8) \quad \frac{d}{dt} \ln \rho(\mathbf{z}(x, t), t) = -\nabla \cdot \mathbf{v}(\mathbf{z}(x, t), t), \ln \rho(\mathbf{z}(x, 0), 0) = \ln \rho_0(x).$$

In fact, when the dimension is very high, since ρ_0 is a positive number very close to 0, there will be a numerical overflow problem when solving equation (2.7), so what we actually solve is equation (2.8).

Together with the Lagrangian method (2.6) and (2.7), this leads to an optimization problem with respect to the velocity field \mathbf{v} , which we will model with a neural network. In addition, we use the Monte Carlo method for integration and suppose x_1, x_2, \dots, x_r are samples drawn from ρ_0 . Along the characteristics, the density satisfies

$$(2.9) \quad \rho(\mathbf{z}(x, t), t) \det(\nabla \mathbf{z}(x, t)) = \rho_0(x)$$

for all $t \in [0, 1]$. Thus,

$$\begin{aligned} \mathcal{E}(\rho, \mathbf{v}) &= \int_0^1 \int_{\Omega} |\mathbf{v}(x, t)|^2 \rho(x, t) dx dt \\ &= \int_0^1 \int_{\Omega} |\mathbf{v}(\mathbf{z}(x, t), t)|^2 \rho(\mathbf{z}(x, t), t) \det(\nabla \mathbf{z}(x, t)) dx dt \\ &= \int_0^1 \int_{\Omega} |\mathbf{v}(\mathbf{z}(x, t), t)|^2 \rho_0(x) dx dt \\ &= \int_0^1 \mathbb{E}_{\mathbf{x} \sim \rho_0} [|\mathbf{v}(\mathbf{z}(\mathbf{x}, t), t)|^2] dt \\ &\approx \int_0^1 \sum_{i=1}^r \frac{1}{r} |\mathbf{v}(\mathbf{z}(x_i, t), t)|^2 dt. \end{aligned}$$

Similarly, we can get

$$\begin{aligned}
\mathcal{P}(\rho) &= \lambda \int_{\Omega} \rho(x, 1) \log \frac{\rho(x, 1)}{\rho_1(x)} dx \\
&= \lambda \int_{\Omega} \log \frac{\rho(\mathbf{z}(x, 1))}{\rho_1(\mathbf{z}(x, 1))} \rho(\mathbf{z}(x, 1), 1) \det(\nabla \mathbf{z}(x, 1)) dx \\
&= \lambda \int_{\Omega} \log \frac{\rho(\mathbf{z}(x, 1))}{\rho_1(\mathbf{z}(x, 1))} \rho_0(x) dx \\
&= \lambda \mathbb{E}_{\mathbf{x} \sim \rho_0} \left[\log \frac{\rho(\mathbf{z}(\mathbf{x}, 1))}{\rho_1(\mathbf{z}(\mathbf{x}, 1))} \right] \\
&\approx \lambda \sum_{i=1}^r \frac{1}{r} \log \frac{\rho(\mathbf{z}(x_i, 1))}{\rho_1(\mathbf{z}(x_i, 1))}.
\end{aligned}$$

Suppose that y_1, y_2, \dots, y_s are samples drawn from a uniform distribution whose density is $P_0(y) = P_0$, which is a constant on the support set of the uniform distribution.

$$\begin{aligned}
\mathcal{R}(\mathbf{v}) &= \alpha \int_0^1 \int_{\Omega} |\nabla \mathbf{v}(x, t)|_F^2 dx dt \\
&= \alpha \int_0^1 \mathbb{E}_{\mathbf{y} \sim P_0} \left[\frac{|\nabla \mathbf{v}(\mathbf{y}, t)|_F^2}{P_0(\mathbf{y})} \right] dt \\
&\approx \frac{\alpha}{sP_0} \int_0^1 \sum_{j=1}^s |\nabla \mathbf{v}(y_j, t)|_F^2 dt.
\end{aligned}$$

Accordingly, we get the following semi-discretization version of OT problem:

$$(2.10) \quad \min_{\mathbf{v}} \bar{\mathcal{F}}(\mathbf{v}, \rho) := \bar{\mathcal{E}}(\mathbf{v}, \rho) + \bar{\mathcal{P}}(\rho) + \bar{\mathcal{R}}(\mathbf{v}),$$

where $\bar{\mathcal{E}}(\mathbf{v}, \rho)$, $\bar{\mathcal{P}}(\rho)$ and $\bar{\mathcal{R}}(\mathbf{v})$ are the discretization versions of $\mathcal{E}(\mathbf{v}, \rho)$, $\mathcal{P}(\rho)$ and $\mathcal{R}(\mathbf{v})$ in the space direction respectively, i.e.,

$$(2.11) \quad \bar{\mathcal{E}}(\mathbf{v}, \rho) := \int_0^1 \sum_{i=1}^r \frac{1}{r} |\mathbf{v}(\mathbf{z}(x_i, t), t)|^2 dt,$$

$$(2.12) \quad \bar{\mathcal{P}}(\rho) := \lambda \sum_{i=1}^r \frac{1}{r} \log \frac{\rho(\mathbf{z}(x_i, 1))}{\rho_1(\mathbf{z}(x_i, 1))},$$

$$(2.13) \quad \bar{\mathcal{R}}(\mathbf{v}) := \frac{\alpha}{sP_0} \int_0^1 \sum_{j=1}^s |\nabla \mathbf{v}(y_j, t)|_F^2 dt,$$

where $\rho(\mathbf{z}(x_i, t), t)$ can be obtained from the solution of (2.8) along the characteristics $\mathbf{z}(x_i, t)$. Then, (2.6) and (2.8) can be reformulated as the following constraints:

$$(2.14) \quad \frac{d}{dt} \mathbf{z}(x_i, t) = \mathbf{v}(\mathbf{z}(x_i, t), t), \quad \mathbf{z}(x_i, 0) = x_i, \quad x_i \sim \rho_0(x_i),$$

$$(2.15) \quad \frac{d}{dt} \ln \rho(\mathbf{z}(x_i, t), t) = -\nabla \cdot \mathbf{v}(\mathbf{z}(x_i, t), t), \quad \ln \rho(\mathbf{z}(x_i, 0), 0) = \ln \rho_0(x_i).$$

2.3.1. Importance Sampling. When the distribution ρ_0 is complex and difficult to sample, or when we want to use the information of the whole region, we can

sample from another distribution μ_0 , such as uniform distribution. At this time, we need to solve one more ODE

$$\frac{d}{dt} \ln \mu(\mathbf{z}(x_i, t), t) = -\nabla \cdot \mathbf{v}(\mathbf{z}(x_i, t), t), \quad \ln \mu(\mathbf{z}(x_i, 0), 0) = \ln \mu_0(x_i).$$

Accordingly, the objective functions are modified to

$$\begin{aligned} \bar{\mathcal{E}}(\mathbf{v}, \rho) &= \int_0^1 \sum_{i=1}^r w_i(t) |\mathbf{v}(\mathbf{z}(x_i, t), t)|^2 dt, \\ \bar{\mathcal{P}}(\rho) &= \lambda \sum_{i=1}^r w_i(1) \log \frac{\rho(\mathbf{z}(x_i, 1), 1)}{\rho_1(\mathbf{z}(x_i, 1))}, \end{aligned}$$

where

$$w_i(t) = \frac{\rho(\mathbf{z}(x_i, t), t)}{\mu(\mathbf{z}(x_i, t), t)r}.$$

2.4. Gradient Calculation. In this paper, we parameterize the velocity field \mathbf{v} by using a neural network $\mathbf{v}(x, t; \theta)$, where θ denotes the trainable parameters. The structure of the neural network will be discussed in the next section. Then, the original optimization problem for the velocity field \mathbf{v} (2.10) can be changed into a deep learning problem. Next, in order to calculate the gradient of the loss function with respect to θ , we have adopted two different methods: the back propagation method and the adjoint state method, which correspond to the discrete-then-optimize and optimize-then-discrete [19, 34], respectively. Gholami et al. [19] and Onken et al. [34] give a thorough discussion of the difference between the discretize-then-optimize and optimize-then-discretize approaches and suggest that the discretize-then-optimize approach is preferable due to the guaranteed accuracy of gradients. In Section 2.4.2 and 3.1, we introduce the adjoint state method and compare it with the back propagation method in numerical experiments for the Gaussian problem. Our experiments show that the back propagation method can achieve superior results to the adjoint state method at reduced computational costs, which aligns with the results achieved in [19] and [34].

2.4.1. Back Propagation. In the discrete-then-optimize method, back propagation is realized by using automatic differentiation, which traverses the computational graph backward in time and is used commonly in machine learning frameworks. Actually, the discretization of the forward propagation completely determines this process.

Since (2.10) is the semi-discretization objective function, we can simplify it as

$$(2.16) \quad \bar{\mathcal{F}}(\theta) = \int_0^1 f(t; \theta) dt + \lambda \sum_{i=1}^r w_i(1) \log \frac{\rho(\mathbf{z}(x_i, 1), 1)}{\rho_1(\mathbf{z}(x_i, 1))},$$

where

$$f(t; \theta) = \sum_{i=1}^r w_i(t) |\mathbf{v}(\mathbf{z}(x_i, t), t; \theta)|^2 + \frac{\alpha}{sP_0} \sum_{j=1}^s |\nabla \mathbf{v}(y_j, t; \theta)|_F^2.$$

We use the composite Simpson formula to discrete the semi-discretization objective function (2.16).

$$\int_0^1 f(t) dt = \sum_{n=0}^{N-1} \int_{t_n}^{t_{n+1}} f(t) dt \approx \frac{h}{6} \sum_{n=0}^{N-1} [f(t_n) + 4f(t_n + \frac{h}{2}) + f(t_{n+1})],$$

where $h = \frac{1}{N}$, $t_n = nh$, $n = 0, \dots, N$.

Next, we perform the fourth-order explicit Runge-Kutta scheme (RK4) to solve ODE constraints (2.14) and (2.15). Then, we can further adopt the Simpson formula to calculate the loss function $\bar{\mathcal{F}}(\theta)$ from (2.16). Finally, the automatic differentiation technique can be used to compute the gradients with respect to the network parameters $\frac{\partial \bar{\mathcal{F}}}{\partial \theta}$, which will be used to update θ . The computational flow chart for calculating the gradients using the back propagation method is shown in Figure 2.1. Then, the parameters θ in the neural network can be optimized by some popular optimizor, such as SGD, Adam, BFGS and so on.

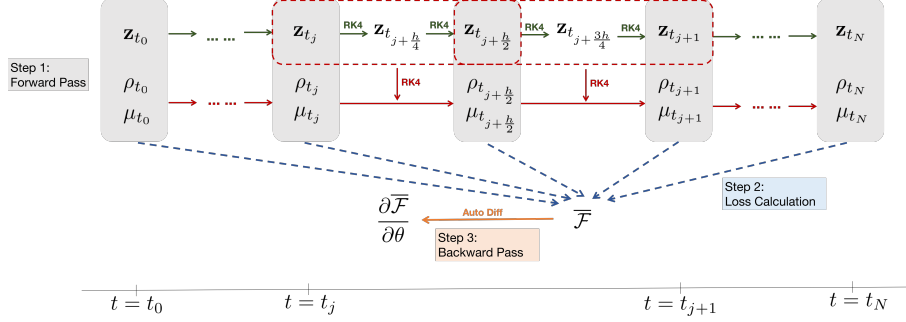


FIG. 2.1. The illustration of the back propagation algorithm.

2.4.2. Adjoint State Method. The discrete-then-optimizer method is common in neural networks and the back propagation is easy to implement, especially when automatic differentiation can be used. However, the back propagation can be memory inefficient because of the potentially huge computation graph. In order to efficiently calculate the gradient $\frac{\partial \bar{\mathcal{F}}}{\partial \theta}$, the optimizer-then-discrete approach, i.e. the adjoint state method has also been introduced in this section. In the adjoint state method, the gradients are computed by numerically solving the adjoint equation. In all of the experiment in this section, we sample x_i drawn from ρ_0 , thus $\omega_i(t) = \frac{1}{r}$, $\forall t \in [0, 1]$, $i = 1, \dots, r$. We can show the gradient calculation in the following proposition.

PROPOSITION 2.1. If $\mu_0 = \rho_0$, the gradient of $\bar{\mathcal{F}}(\theta)$ is calculated by the formula

$$(2.17) \quad \begin{aligned} \frac{\partial \bar{\mathcal{F}}(\theta)}{\partial \theta} = & \frac{1}{r} \sum_{i=1}^r \int_0^1 [(2\mathbf{v}(\mathbf{z}_i(t), t; \theta) - U_i(t))^T \mathbf{v}_\theta(\mathbf{z}_i(t), t; \theta) - \lambda \nabla \cdot \mathbf{v}_\theta(\mathbf{z}_i(t), t; \theta)] dt \\ & + \frac{\alpha}{sP_0} \sum_{j=1}^s \int_0^1 2 \langle \nabla \mathbf{v}_\theta(y_j, t; \theta), \nabla \mathbf{v}(y_j, t) \rangle dt. \end{aligned}$$

Here we denote $\mathbf{z}(x_i, t)$ by $\mathbf{z}_i(t)$ for simplification. Moreover, $\langle \cdot, \cdot \rangle$ is defined as

$$\langle A, B \rangle = \sum_{i,j} A_{i,j} B_{i,j}$$

and A, B are two matrices with the same size. $U_i(t)$ is the solution of the adjoint

equation

$$(2.18) \quad \begin{cases} \frac{dU_i(t)}{dt} + \nabla^T \mathbf{v}(\mathbf{z}_i(t), t) U_i(t) = [2(\nabla \mathbf{v})^T \mathbf{v} - \lambda \nabla(\nabla \cdot \mathbf{v})](\mathbf{z}_i(t), t; \theta), \\ U(1) = \lambda \frac{\nabla \rho_1(\mathbf{z}_i(1))}{\rho_1(\mathbf{z}_i(1))}. \end{cases}$$

The detailed proof of the above proposition is shown in Supplementary Materials. For the adjoint state method, the computation of the gradients follows three steps: forward pass, backward pass and gradient calculation, which are different from the back propagation method. Firstly, the forward pass is realized by using the fourth-order explicit Runge-Kutta scheme only to solve (2.14) to get the activation throughout time $\mathbf{z}(t)$. Then, the terminal value condition of the adjoint ODE, $U_{t_N} = U(t = 1)$, can be further computed by plugging in the values for $\mathbf{z}_{t_N} = \mathbf{z}(t = 1)$. During the backward pass, we need to solve the adjoint ODE (2.18) to compute $U(t)$ by using all activations $\mathbf{z}(t)$ and still adopting the fourth-order explicit Runge-Kutta scheme. Finally, the gradient with respect to the network parameters $\frac{\partial \bar{\mathcal{F}}}{\partial \theta}$ can be computed by using $\mathbf{z}(t)$ and $U(t)$ from (2.17). The computational flow chart for calculating the gradients using the adjoint state method is shown in Figure 2.2. It is worth to mention that in order to reduce the memory storage for storing intermediate activations $\mathbf{z}(t)$, only the activation of the last state $\mathbf{z}(1)$ need to be saved in the forward pass, while the intermediate states $\mathbf{z}(t)$ will be recomputed by solving the forward ODE (2.14) backward in time during the backward pass.

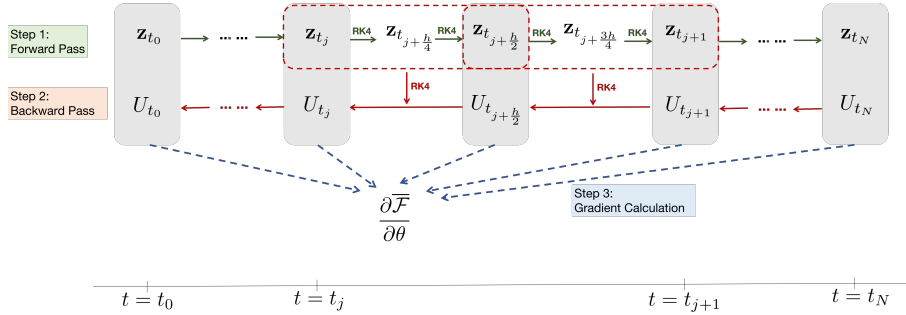


FIG. 2.2. The illustration of the adjoint state method.

2.5. Neural Network Architecture. In order to solve high-dimensional OT problem, we parameterize the velocity field by a neural network, which can naturally lead to a mesh-free scheme by combining Lagrangian method and Monte Carlo integration. We now introduce our neural network parameterization of the velocity field. In the following, we denote our model as

$$\mathbf{v}(x, t; \theta) = \sum_{i=0}^M \mathbf{v}_i(x; \theta) \phi_i(t),$$

where $(x, t) \in \mathbb{R}^{d+1}$ is the input feature, θ is the network parameters and $\phi_i(t)$ is chosen as the nodal basis function in the time direction, i.e.,

$$\phi_i(t) = \begin{cases} 0, & t \leq t_{i-1}, \\ \frac{t-t_{i-1}}{t_i-t_{i-1}} = M(t-t_{i-1}), & t_{i-1} < t \leq t_i, \\ \frac{t_{i+1}-t}{t_{i+1}-t_i} = M(t_{i+1}-t), & t_i < t \leq t_{i+1}, \\ 0, & t > t_{i+1}, \end{cases}$$

and $M+1$ denotes the number of the basis function. When M is fixed, we can choose N (the number of time steps in forward pass) as kM , such as $k = 2$, so that the forward ODEs (2.6) and (2.8) can be solved accurately. Besides, $\mathbf{v}_i(x; \theta)$ is the sum of some two-layer neural networks designed as $\mathbf{v}_i(x; \theta) = \sum_{l=1}^L [W_{2i}^{(l)} \sigma(W_{1i}^{(l)} x + b_{1i}^{(l)}) + b_{2i}^{(l)}]$, $W_{1i}^{(l)} \in \mathbb{R}^{H \times d}$, $W_{2i}^{(l)} \in \mathbb{R}^{d \times H}$, $b_{1i}^{(l)} \in \mathbb{R}^H$, $b_{2i}^{(l)} \in \mathbb{R}^d$, the network parameters $\theta = \{W_{1i}^{(l)}, W_{2i}^{(l)}, b_{1i}^{(l)}, b_{2i}^{(l)}\}$, L is the width of the network and $\sigma(x) = \tanh(x)$ is the activation function. The advantage of the design of our neural network architecture is to reduce the oscillations in the time direction because we use the piecewise linear function to be the basis function.

Next, to demonstrate the effective of the above network design, we compare it experimentally with a more natural network structure:

$$\mathbf{v}^*(x, t; \theta) = \sum_{l=1}^L [W_2^{(l)}(t) \sigma(W_1^{(l)}(t)x + b_1^{(l)}(t)) + b_2^{(l)}(t)]$$

since $W_1^{(l)}(t) \in \mathbb{R}^{H \times d}$, $W_2^{(l)}(t) \in \mathbb{R}^{d \times H}$, $b_1^{(l)}(t) \in \mathbb{R}^H$ and $b_2^{(l)}(t) \in \mathbb{R}^d$ are time dependent and parameterized directly by the nodal basis functions, i.e.

$$W_e^{(l)}(t) = \sum_{i=0}^M W_{ei}^{(l)} \phi_i(t), \quad b_e^{(l)}(t) = \sum_{i=0}^M b_{ei}^{(l)} \phi_i(t) \quad \text{for } e = 1, 2.$$

We have found that these two velocity fields $\mathbf{v}(x, t; \theta)$ and $\mathbf{v}^*(x, t; \theta)$ have different network structures, however, the same number of parameters, i.e., $L(M+1)(2dH + H + d)$. Therefore, in order to compare these two neural networks' architecture fairly and intuitively, we give an example in the 1-dimensional case ($d = 1$) for Gaussian problem. The initial density ρ_0 is a Gaussian with means 0 and variance 0.3, while the target density ρ_1 is a Gaussian with means -4 and variance 1.0. The parameters of the network structure are chosen as $L = 2$, $M = 5$ and $H = 10$ for both velocity fields. We train our networks using 1000 iterations of Adam with a learning rate of 0.01. We visualize the trained velocity field $\mathbf{v}(x, t; \theta)$ and $\mathbf{v}^*(x, t; \theta)$ at $x = -2, 0, 4$ respectively in Figure 2.3. It can be observed that, on the one hand, the velocity field $\mathbf{v}(x, t; \theta)$ is piecewise linear with respect to time, while $\mathbf{v}^*(x, t; \theta)$ is nonlinear with respect to time, on the other hand, the oscillation of velocity field \mathbf{v} in the time direction is obviously smaller than that of the velocity field \mathbf{v}^* , both in terms of frequency and amplitude. The frequency of \mathbf{v} is exactly 5, which is actually equal to M and clearly smaller than the frequency of the velocity field \mathbf{v}^* . In addition, the maximum oscillation amplitude of \mathbf{v} is about 4.5, while the maximum oscillation amplitude of \mathbf{v}^* is about 11. Since we need to solve ODEs in the time direction, it is difficult to control the numerical accuracy if the velocity field oscillates too much, so the velocity field \mathbf{v} is more beneficial to the control accuracy.

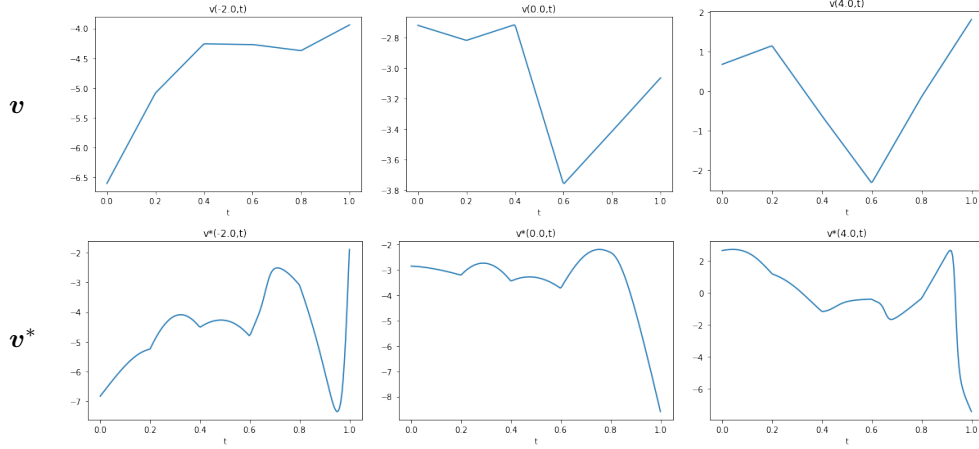


FIG. 2.3. The comparison of network structures \mathbf{v} and \mathbf{v}^* .

2.6. Crowd Motion. Our method can also be easily applied to the crowd motion problem [41]. In contrast to the OT problem, the crowd motion problem not only needs to move the initial density ρ_0 approximately to the target density ρ_1 , but also expects to avoid some obstacles in the dynamic movement. The obstacles can be expressed by introducing an added term to the loss function, i.e. the preference term:

$$(2.19) \quad \mathcal{Q}(\rho) = \lambda_P \int_0^1 \int_{\mathbb{R}^d} Q(x) \rho(x, t) dx dt,$$

where λ_P is the penalty parameter, and $Q : \mathbb{R}^d \rightarrow \mathbb{R}$ models the spatial preferences of agents, i.e. the larger $Q(x)$ is, the closer the position of x is to the obstacles. We can get the following formulation:

$$\min_{(\mathbf{v}, \rho) \in \mathcal{C}(\rho_0, \rho_1)} \mathcal{F}_{cm}(\mathbf{v}, \rho) := \mathcal{E}(\mathbf{v}, \rho) + \mathcal{Q}(\rho),$$

where $\mathcal{E}(\mathbf{v}, \rho)$ and $\mathcal{C}(\rho_0, \rho_1)$ are what we defined in Section 2.1:

$$\begin{aligned} \mathcal{E}(\rho, \mathbf{v}) &= \int_0^1 \int_{\Omega} |\mathbf{v}(x, t)|^2 \rho(x, t) dx dt, \\ \mathcal{C}(\rho_0, \rho_1) &= \{(\rho, \mathbf{v}) : \partial_t \rho + \nabla \cdot (\rho \mathbf{v}) = 0, \rho(\cdot, 0) = \rho_0, \rho(\cdot, 1) = \rho_1\}. \end{aligned}$$

The method to solve the crowd motion problem is almost the same as the OT problem. Firstly, as in Section 2.2, we relax the terminal density as an implicit condition penalized by using KL divergence term \mathcal{P} to get the following problem:

$$(2.20) \quad \min_{(\mathbf{v}, \rho) \in \mathcal{C}(\rho_0)} \mathcal{E}(\mathbf{v}, \rho) + \mathcal{Q}(\rho) + \mathcal{P}(\rho),$$

where

$$\begin{aligned} \mathcal{P}(\rho) &= \lambda \int_{\Omega} \rho(x, 1) \log \frac{\rho(x, 1)}{\rho_1(x)} dx, \\ \mathcal{C}(\rho_0) &= \{(\rho, \mathbf{v}) : \partial_t \rho + \nabla \cdot (\rho \mathbf{v}) = 0, \rho(\cdot, 0) = \rho_0\}. \end{aligned}$$

Then we adopt the Lagrangian discretization method presented in Section 2.2 to get the semi-discrete formulation of (2.20):

$$(2.21) \quad \min_{\mathbf{v}} \bar{\mathcal{E}}(\mathbf{v}, \rho) + \bar{\mathcal{P}}(\rho) + \bar{\mathcal{Q}}(\rho)$$

s.t.

$$(2.22) \quad \frac{d}{dt} \mathbf{z}(x_i, t) = \mathbf{v}(\mathbf{z}(x_i, t), t), \quad \mathbf{z}(x_i, 0) = x_i, \quad x_i \sim \rho_0(x_i),$$

$$(2.23) \quad \frac{d}{dt} \ln \rho(\mathbf{z}(x_i, t), t) = -\nabla \cdot \mathbf{v}(\mathbf{z}(x_i, t), t), \quad \ln \rho(\mathbf{z}(x_i, 0), 0) = \ln \rho_0(x_i),$$

where $\bar{\mathcal{E}}, \bar{\mathcal{P}}$ are defined in (2.11), (2.12) respectively,

$$\begin{aligned} \bar{\mathcal{E}}(\mathbf{v}, \rho) &:= \int_0^1 \sum_{i=1}^r \frac{1}{r} |\mathbf{v}(\mathbf{z}(x_i, t), t)|^2 dt, \\ \bar{\mathcal{P}}(\rho) &:= \lambda \sum_{i=1}^r \frac{1}{r} \log \frac{\rho(\mathbf{z}(x_i, 1), 1)}{\rho_1(\mathbf{z}(x_i, 1))}, \end{aligned}$$

and $\bar{\mathcal{Q}}$ is the semi-discrete version of \mathcal{Q} :

$$\bar{\mathcal{Q}}(\rho) := \int_0^1 \sum_{i=1}^r \frac{1}{r} Q(\mathbf{z}(x_i, t)) dt.$$

The velocity field \mathbf{v} is parameterized by neural network $\mathbf{v}(x, t; \theta)$ discussed in Section 2.5. We discrete (2.21) by the composite Simpson formula and we use the fourth-order explicit Runge-Kutta scheme to solve ODE constraints (2.22) and (2.23). So that back propagation can be naturally used to calculate the gradient of objective function with respect to network parameters in crowd motion problems.

3. Numerical Experiments. In this section, we first compare the performance of the adjoint state method with the back propagation method for Gaussian examples (i.e. the initial and target densities are both Gaussian). Next, we demonstrate the performance of the proposed model and its OT results through some numerical experiments. We compare it with several representative and related numerical methods: the Sinkhorn method [11] and MFGnet [41]. We test the effectiveness of our proposed method in high dimensions on some synthetic test problems, including the Gaussian examples and crowd motion examples to perform quantitative and qualitative comparisons, respectively. All the experiments of our proposed method are implemented in PyTorch on a NVIDIA Tesla V100 GPU with 32GB memory.

3.1. Compare the Adjoint State Method with the Back Propagation.

We consider three typical Gaussian examples with different means and covariance matrices shown in list below. Here $\rho_G(\cdot, \mathbf{m}, \mathbf{\Sigma})$ is the probability density function of a d -variate Gaussian with mean $\mathbf{m} \in \mathbb{R}^d$ and covariance matrix $\mathbf{\Sigma} \in \mathbb{R}^{d \times d}$. Since the initial density ρ_0 and the target density ρ_1 are both Gaussian functions, the ground truth of the transport costs for the OT problem can be exactly known [37].

- Test 1: $\rho_0(x) = \rho_G(x, \mathbf{0}, \mathbf{I})$, $\rho_1(x) = \rho_G(x, -4 \cdot \mathbf{e}_1, \mathbf{I})$
- Test 2: $\rho_0(x) = \rho_G(x, \mathbf{0}, 0.3 \cdot \mathbf{I})$, $\rho_1(x) = \rho_G(x, -4 \cdot \mathbf{e}_1, \mathbf{I})$
- Test 3: $\rho_0(x) = \rho_G(x, -4 \cdot \mathbf{e}_1 - 4 \cdot \mathbf{e}_2, \mathbf{I})$, $\rho_1(x) = \rho_G(x, 4 \cdot \mathbf{e}_1 + 4 \cdot \mathbf{e}_2, \mathbf{I})$

In this section, we compare the adjoint state method with the back propagation method for Gaussian examples. For both methods, the fourth-order explicit Runge-Kutta scheme with a fixed step size is used to solve ODEs and the Simpson formula is adopted for integration in time direction. Besides, for fair comparison, the adjoint state method and the back propagation method use the same structure of the neural network, the same number of time steps and the same learning rate for all the experiments.

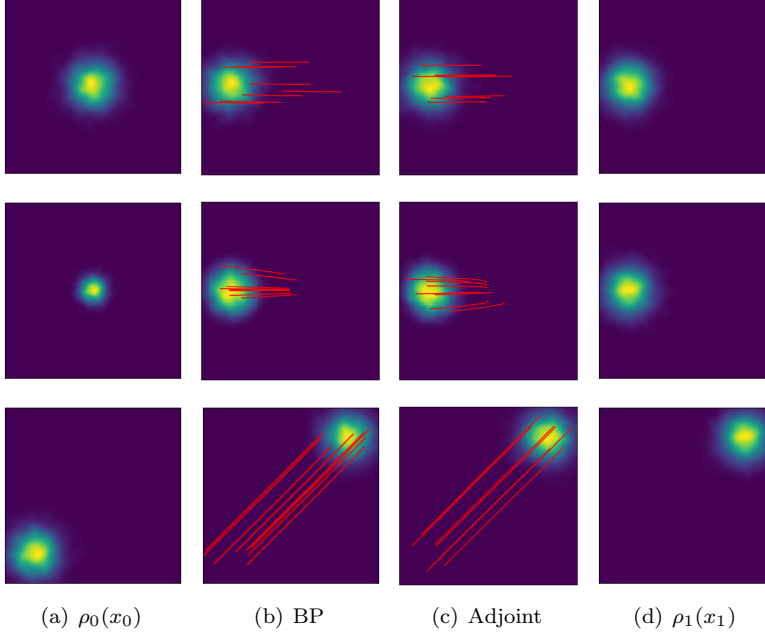


FIG. 3.1. *BP v.s. adjoint state method.*

In Figure 3.1, we show the experiments results of the back propagation method (b) and the adjoint state method (c) in dimension 2. It can be observed that the push forward of ρ_0 are very similar to the target density ρ_1 for both compared approaches, however, the characteristics are not straight enough for the adjoint state method, especially for Test 2.

TABLE 3.1
The comparison of BP and adjoint state method in dimension 2.

Transport costs	Test 1	Test 2	Test 3
BP	15.8792	16.3305	127.7931
Adjoint	15.8792	18.1147	128.8924
Ground truth	16.0000	16.4091	128.0000

For better comparison, the average values of transport cost obtained with these two methods are also compared in Table 3.1. We can clearly observe that the transport cost estimated by the back propagation is more closer to the ground truth than the results of the adjoint state method. The back propagation method shows better

performance than the adjoint state method both quantitatively and qualitatively. Therefore, in the later experiments, we all use the back propagation method.

3.2. Gaussian Examples. In Table 3.2, the average transport costs over five seeds have been calculated and recorded for each method. We can clearly see that the proposed method and MFGnet can lead to better quantitative results than the Sinkhorn method, especially when the dimension is very high.

TABLE 3.2
Transport costs of these three instances for different methods in $d = 2, 10, 50$.

Transport costs	Test 1	Test 2	Test 3
$d = 2$			
Sinkhorn	16.1087	16.4795	127.3440
MFGnet	15.7212	16.3645	127.9155
Ours(BP)	15.8792	16.3305	127.7931
Ground truth	16.0000	16.4091	128.0000
$d = 10$			
Sinkhorn	18.5652	19.4240	130.5551
MFGnet	15.6780	18.0464	127.9691
Ours(BP)	16.0131	17.9837	128.1140
Ground truth	16.0000	18.0455	128.0000
$d = 50$			
Sinkhorn	62.1359	51.4754	174.1247
MFGnet	-	-	-
Ours(BP)	16.1800	26.0273	128.2735
Ground truth	16.0000	26.2270	128.0000

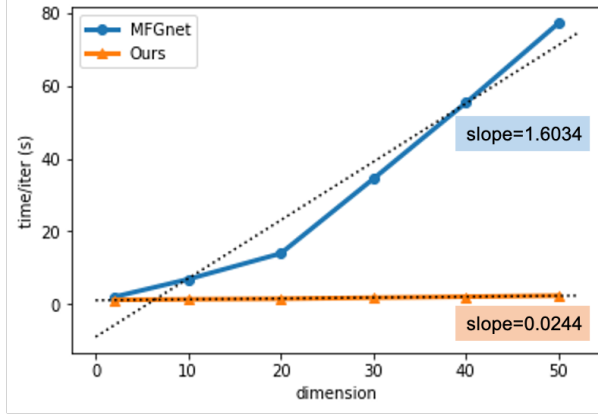


FIG. 3.2. The computational time of each iteration in different dimensions. For MFGnet, the number of training samples are: 2304, 6400, 8464, 10816, 13456 and 16384 at $d = 2, 10, 20, 30, 40$ and 50 , respectively. For the proposed method, 1024 is chosen for all dimensional cases.

Note that, for using the Sinkhorn method, firstly, we should discrete the Gaussian distribution by Monte Carlo sampling (see Supplementary Materials for additional experiments of Sinkhorn). Besides, for MFGnet, as the dimension increases, the

number of training samples are chosen as 2304, 6400 and 16384 for the 2, 10 and 50 dimensional cases, respectively, as recommended in the literature [41]. Indeed, the running time at dimension 50 is more than 20 hours for each experiment and the BFGS method used in [41] sometimes fails in the line search, therefore the results are marked with the symbol “-” in Table 3.2. In addition, we can observe from Figure 3.2 that the computational time of MFGnet will greatly increase and the slope of growth is about 1.6034. For the proposed method, the number of training samples is set as 1024 for all dimensions, and the computational efficiency is only slightly influenced by the increase in dimension (see Figure 3.2). The growth slope of the proposed method is only 0.0244, which is much lower than MFGnet. These experiments demonstrate that the proposed method is faster and more efficient than MFGnet and Sinkhorn methods for high-dimensional dynamic OT problems.

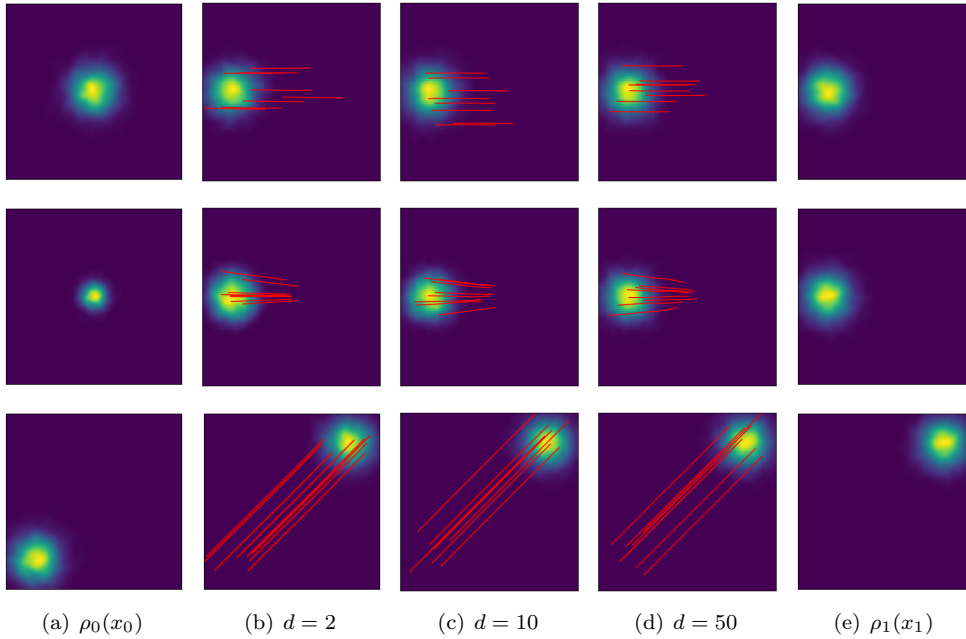


FIG. 3.3. The density evolution of Gaussian examples.

Next, for better illustration, we also show the density evolution of the proposed method moving from the initial distribution to the target one in Figure 3.3. The first column (a) and the last (e) column of Figure 3.3 show the initial density ρ_0 and the target density ρ_1 , respectively. The other columns ((b)-(d)) correspond to the results of the push forward of the initial density ρ_0 in dimension $d = 2, 10$ and 50 , respectively. We can clearly see that the target density estimated by our trained network shown in (b)-(d) are very similar to the target density ρ_1 , both in the means and covariance matrices, for all these high-dimensional instances. Note that for $d > 2$, we just show slices along the first two coordinate directions. Besides, the red lines represent the characteristics (i.e. the learned trajectories) starting from randomly sampled points according to the initial density ρ_0 . It can be observed that the characteristics are almost straight lines, which conforms the density movement is reasonable and the training is successful.

3.3. Crowd Motion Examples. In this section, we mainly consider the crowd motion problem which is a generalization of the optimal transport problem. In particular, when $\lambda_P = 0$ in (2.19), the crowd motion problem will degenerate into an OT problem.

In list below, we list two representative tests with different choices of initial density ρ_0 , target density ρ_1 and preference function $Q(x)$ is Gaussian or Gaussian mixture, corresponding to one obstacle (Test 4) and two obstacles (Test 5) respectively. Note that for $d > 2$, we just use the first two components of x to evaluate the preference function $Q(x)$.

- Test4: $\rho_0(x) = \rho_G(x, -3 \cdot \mathbf{e}_1, 0.3 \cdot \mathbf{I})$, $\rho_1(x) = \rho_G(x, 3 \cdot \mathbf{e}_1, 0.3 \cdot \mathbf{I})$,
 $Q(x) = \rho_G(x, \mathbf{0}, \text{diag}(0.5, 1))$
- Test5: $\rho_0(x) = \rho_G(x, -4 \cdot \mathbf{e}_1, 0.3 \cdot \mathbf{I})$, $\rho_1(x) = \rho_G(x, 4 \cdot \mathbf{e}_1, 0.3 \cdot \mathbf{I})$,
 $Q(x) = \frac{1}{2}\rho_G(x, -2 \cdot \mathbf{e}_2, \text{diag}(0.1, 1)) + \frac{1}{2}\rho_G(x, 2 \cdot \mathbf{e}_2, \text{diag}(0.1, 1))$

We set the main parameters as $\lambda = 10$, $\lambda_P = 500$ and $\alpha = 0$ and we focus on the case $d = 2$ (left two columns) and $d = 5$ (right two columns) in Figure 3.4. The last row shows the obstacles in the center of the domain and the red lines present the learned characteristics. The remaining rows in Figure 3.4 show the density evolution at intermediate time $t = \frac{1}{5}, \frac{1}{2}, \frac{4}{5}, 1$ from the initial density ρ_0 to the target density ρ_1 . We can clearly observe that the push forward of ρ_0 (i.e. $\tilde{\rho}_1(\tilde{x}_1)$) is similar to the target density ρ_1 and the characteristics are curved, not straight, to avoid the regions where these obstacles are located.

Our second crowd motion experiment simulates some maze examples in Figure 3.5 and obstacles are represented by an indicator function where the regions are regular rectangles. We show the crowd motion results of two-dimensional case with different obstacles. In order to avoid obstacles successfully, firstly, we adopt the same method as Gaussian function to blur rectangular obstacles properly shown in the last row of Figure 3.5. Different colors indicate the strength of the obstruction in different parts of the obstacles, that is, the darker the color, the smaller the obstruction. The density evolution and characteristics show that the mass can circumvent the obstacles very well, which demonstrates the success of our algorithm in the crowd motion problem.

4. Conclusion. Motivated by the fact that the traditional mesh-based discretization method usually leads to the curse of dimensionality, we propose a novel neural network based method for solving dynamic OT problems effectively in very high-dimensional spaces. In order to calculate the gradient accurately, we have adopted two different method: the back propagation method and the adjoint state method. The numerical experiments demonstrate that the proposed back propagation method performs well compared to the MFGnet and the Sinkhorn method. Our proposed method is easy to implement and high precision in experiments. Generally speaking, for different dimension, our proposed method takes about 1.5s to perform one iteration with our unoptimized PyTorch codes and GPU implementation. In the future, we will further study how to extend this method to the unnormalized OT problems, which means initial and target densities with different total mass.

REFERENCES

- [1] O. ABDEL-HAMID, A.-R. MOHAMED, H. JIANG, L. DENG, G. PENN, AND D. YU, *Convolutional neural networks for speech recognition*, IEEE/ACM Transactions on Audio, Speech, and Language Processing, 22 (2014), pp. 1533–1545.

- [2] B. AMOS, L. XU, AND J. Z. KOLTER, *Input convex neural networks*, in International Conference on Machine Learning, 2017, pp. 146–155.
- [3] D. AN, Y. GUO, N. LEI, Z. LUO, S.-T. YAU, AND X. GU, *Ae-ot: a new generative model based on extended semi-discrete optimal transport*, in International Conference on Learning Representations 2020, 2019.
- [4] D. AN, Y. GUO, M. ZHANG, X. QI, N. LEI, AND X. GU, *Ae-ot-gan: Training gans from data specific latent distribution*, in European Conference on Computer Vision, Springer, 2020, pp. 548–564.
- [5] M. ARJOVSKY, S. CHINTALA, AND L. BOTTOU, *Wasserstein gan*, arXiv:1701.07875, (2017).
- [6] J.-D. BENAMOU AND Y. BRENIER, *A computational fluid mechanics solution to the Monge-Kantorovich mass transfer problem*, Numerische Mathematik, 84 (2000), pp. 375–393.
- [7] J.-D. BENAMOU, B. D. FROESE, AND A. M. OBERMAN, *Numerical solution of the optimal transportation problem using the Monge–Ampère equation*, Journal of Computational Physics, 260 (2014), pp. 107–126.
- [8] Y. BRENIER, *Polar factorization and monotone rearrangement of vector-valued functions*, Communications on Pure and Applied Mathematics, 44 (1991), pp. 375–417.
- [9] R. COLLOBERT AND J. WESTON, *A unified architecture for natural language processing: Deep neural networks with multitask learning*, in Proceedings of the 25th international conference on Machine learning, 2008, pp. 160–167.
- [10] N. COURTY, R. FLAMARY, D. TUIA, AND A. RAKOTOMAMONJY, *Optimal transport for domain adaptation*, IEEE Transactions on Pattern Analysis and Machine Intelligence, 39 (2017), pp. 1853–1865.
- [11] M. CUTURI, *Sinkhorn distances: Lightspeed computation of optimal transport*, Advances in Neural Information Processing Systems, 26 (2013), pp. 2292–2300.
- [12] L. DENG, G. HINTON, AND B. KINGSBURY, *New types of deep neural network learning for speech recognition and related applications: An overview*, in 2013 IEEE International Conference on Acoustics, Speech and Signal Processing, IEEE, 2013, pp. 8599–8603.
- [13] R. DEVORE, B. HANIN, AND G. PETROVA, *Neural network approximation*, Acta Numerica, 30 (2021), pp. 327–444.
- [14] W. E, J. HAN, AND A. JENTZEN, *Deep learning-based numerical methods for high-dimensional parabolic partial differential equations and backward stochastic differential equations*, Communications in Mathematics and Statistics, 5 (2017), pp. 349–380.
- [15] W. E AND B. YU, *The deep ritz method: a deep learning-based numerical algorithm for solving variational problems*, Communications in Mathematics and Statistics, 6 (2018), pp. 1–12.
- [16] C. FINLAY, J.-H. JACOBSEN, L. NURBEKYAN, AND A. OBERMAN, *How to Train Your Neural ODE: The World of Jacobian and Kinetic Regularization*, in Proceedings of the 37th International Conference on Machine Learning, PMLR, Nov. 2020, pp. 3154–3164.
- [17] W. GANGBO, W. LI, S. OSHER, AND M. PUTHAWALA, *Unnormalized optimal transport*, Journal of Computational Physics, 399 (2019), p. 108940.
- [18] A. GENEVAY, M. CUTURI, G. PEYRÉ, AND F. BACH, *Stochastic optimization for large-scale optimal transport*, in Proceedings of the 30th International Conference on Neural Information Processing Systems, 2016, p. 3440–3448.
- [19] A. GHOLAMI, K. KEUTZER, AND G. BIROS, *Anode: Unconditionally accurate memory-efficient gradients for neural odes*, in International Joint Conferences on Artificial Intelligence (IJCAI), 2019.
- [20] Y. GOLDBERG, *A primer on neural network models for natural language processing*, Journal of Artificial Intelligence Research, 57 (2016), pp. 345–420.
- [21] I. GOODFELLOW, Y. BENGIO, AND A. COURVILLE, *Deep Learning*, MIT Press, 2016. <http://www.deeplearningbook.org>.
- [22] X. GU, F. LUO, J. SUN, AND S. T. YAU, *Variational principles for minkowski type problems, discrete optimal transport, and discrete monge-ampere equations*, Asian Journal of Mathematics, 20 (2016), pp. 383–398.
- [23] M. HENRY, E. MAITRE, AND V. PERRIER, *Primal-dual formulation of the dynamic optimal transport using Helmholtz-Hodge decomposition*. 2019.
- [24] L. KANTOROVICH, *On the translocation of masses*, Management Science, 5 (1958), pp. 1–4.
- [25] A. KRIZHEVSKY, I. SUTSKEVER, AND G. E. HINTON, *Imagenet classification with deep convolutional neural networks*, Advances in neural information processing systems, 25 (2012), pp. 1097–1105.
- [26] M. KUSNER, Y. SUN, N. KOLKIN, AND K. WEINBERGER, *From word embeddings to document distances*, in International conference on machine learning, PMLR, 2015, pp. 957–966.
- [27] J.-M. LASRY AND P.-L. LIONS, *Mean field games*, Japanese Journal of Mathematics, 2 (2007), pp. 229–260.

- [28] N. LEI, K. SU, L. CUI, S.-T. YAU, AND X. D. GU, *A geometric view of optimal transportation and generative model*, Computer Aided Geometric Design, 68 (2019), pp. 1–21.
- [29] M. LINDSEY AND Y. A. RUBINSTEIN, *Optimal transport via a Monge-Ampère optimization problem*, SIAM Journal on Mathematical Analysis, 49 (2017), pp. 3073–3124.
- [30] J. LIU, W. YIN, W. LI, AND Y. T. CHOW, *Multilevel optimal transport: a fast approximation of Wasserstein-1 distances*, SIAM Journal on Scientific Computing, 43 (2021), pp. A193–A220.
- [31] J. LU, Z. SHEN, H. YANG, AND S. ZHANG, *Deep network approximation for smooth functions*, SIAM Journal on Mathematical Analysis, 53 (2021), pp. 5465–5506.
- [32] A. V. MAKKUA, A. TAGHVAEI, S. OH, AND J. LEE, *Optimal transport mapping via input convex neural networks*, in Proceedings of the 37th International Conference on Machine Learning, 2020, pp. 6672–6681.
- [33] G. MONGE, *Mémoire sur la théorie des déblais et des remblais*, Histoire de l’Académie Royale des Sciences, (1781).
- [34] D. ONKEN AND L. RUTHOTTO, *Discretize-optimize vs. optimize-discretize for time-series regression and continuous normalizing flows*, arXiv: 2005.13420, (2020).
- [35] N. PAPADAKIS, *Optimal transport for image processing*, PhD thesis, Université de Bordeaux; Habilitation thesis, 2015.
- [36] N. PAPADAKIS, G. PEYRÉ, AND E. OUDET, *Optimal transport with proximal splitting*, SIAM Journal on Imaging Sciences, 7 (2014), pp. 212–238.
- [37] G. PEYRÉ AND M. CUTURI, *Computational and trends in machine learning*, Foundations and Trends in Machine Learning, (2019), pp. 355–607.
- [38] C. R. PRINS, R. BELTMAN, J. H. M. TEN THIJE BOONKAMP, W. L. IJZERMAN, AND T. W. TUKKER, *A least-squares method for optimal transport using the Monge-Ampère equation*, SIAM Journal on Scientific Computing, 37 (2015), pp. B937–B961.
- [39] M. RAISSI, P. PERDIKARIS, AND G. E. KARNIADAKIS, *Physics-informed neural networks: A deep learning framework for solving forward and inverse problems involving nonlinear partial differential equations*, Journal of Computational Physics, 378 (2019), pp. 686–707.
- [40] I. REDKO, N. COURTY, R. FLAMARY, AND D. TUIA, *Optimal transport for multi-source domain adaptation under target shift*, arXiv:1803.04899, (2019).
- [41] L. RUTHOTTO, S. J. OSHER, W. LI, L. NURBEKYAN, AND S. W. FUNG, *A machine learning framework for solving high-dimensional mean field game and mean field control problems*, Proceedings of the National Academy of Sciences of the United States of America, 117 (2020), pp. 9183–9193.
- [42] T. SALIMANS, H. ZHANG, A. RADFORD, AND D. METAXAS, *Improving gans using optimal transport*, arXiv:1803.05573, (2018).
- [43] F. SANTAMBROGIO, *Optimal transport for applied mathematicians*, Birkhäuser, Cham, 2015.
- [44] J. SCHMIDHUBER, *Deep learning in neural networks: An overview*, Neural networks, 61 (2015), pp. 85–117.
- [45] V. SEGUY, B. B. DAMODARAN, R. FLAMARY, N. COURTY, A. ROLET, AND M. BLONDEL, *Large scale optimal transport and mapping estimation*, in International Conference on Learning Representations, 2018.
- [46] Z. SHEN, H. YANG, AND S. ZHANG, *Neural network approximation: Three hidden layers are enough*, Neural Networks, 141 (2021), pp. 160–173.
- [47] R. SINKHORN, *A relationship between arbitrary positive matrices and doubly stochastic matrices*, Annals of Mathematical Statistics, 35 (1964), pp. 876–879.
- [48] J. SIRIGNANO AND K. SPILIOPOULOS, *DGM: A deep learning algorithm for solving partial differential equations*, Journal of Computational Physics, 375 (2018), pp. 1339–1364.
- [49] F. SULTANA, A. SUFIAN, AND P. DUTTA, *Advancements in image classification using convolutional neural network*, in 2018 Fourth International Conference on Research in Computational Intelligence and Communication Networks (ICRCICN), IEEE, 2018, pp. 122–129.
- [50] A. TONG, J. HUANG, G. WOLF, D. V. DIJK, AND S. KRISHNASWAMY, *Trajectorynet: A dynamic optimal transport network for modeling cellular dynamics*, in Proceedings of the 37th International Conference on Machine Learning, 2020.
- [51] L. C. TORRES, L. M. PEREIRA, AND M. H. AMINI, *A survey on optimal transport for machine learning: Theory and applications*, arXiv:2106.01963, (2021).
- [52] C. VILLANI, *Topics in optimal transportation*, vol. 58, American Mathematical Society, 2003.
- [53] ———, *Optimal transport: old and new*, vol. 338, Springer-Verlag, Berlin, 2009.
- [54] J. YU, R. LAI, W. LI, AND S. OSHER, *A fast proximal gradient method and convergence analysis for dynamic mean field planning*, arXiv:2102.13260, (2021).

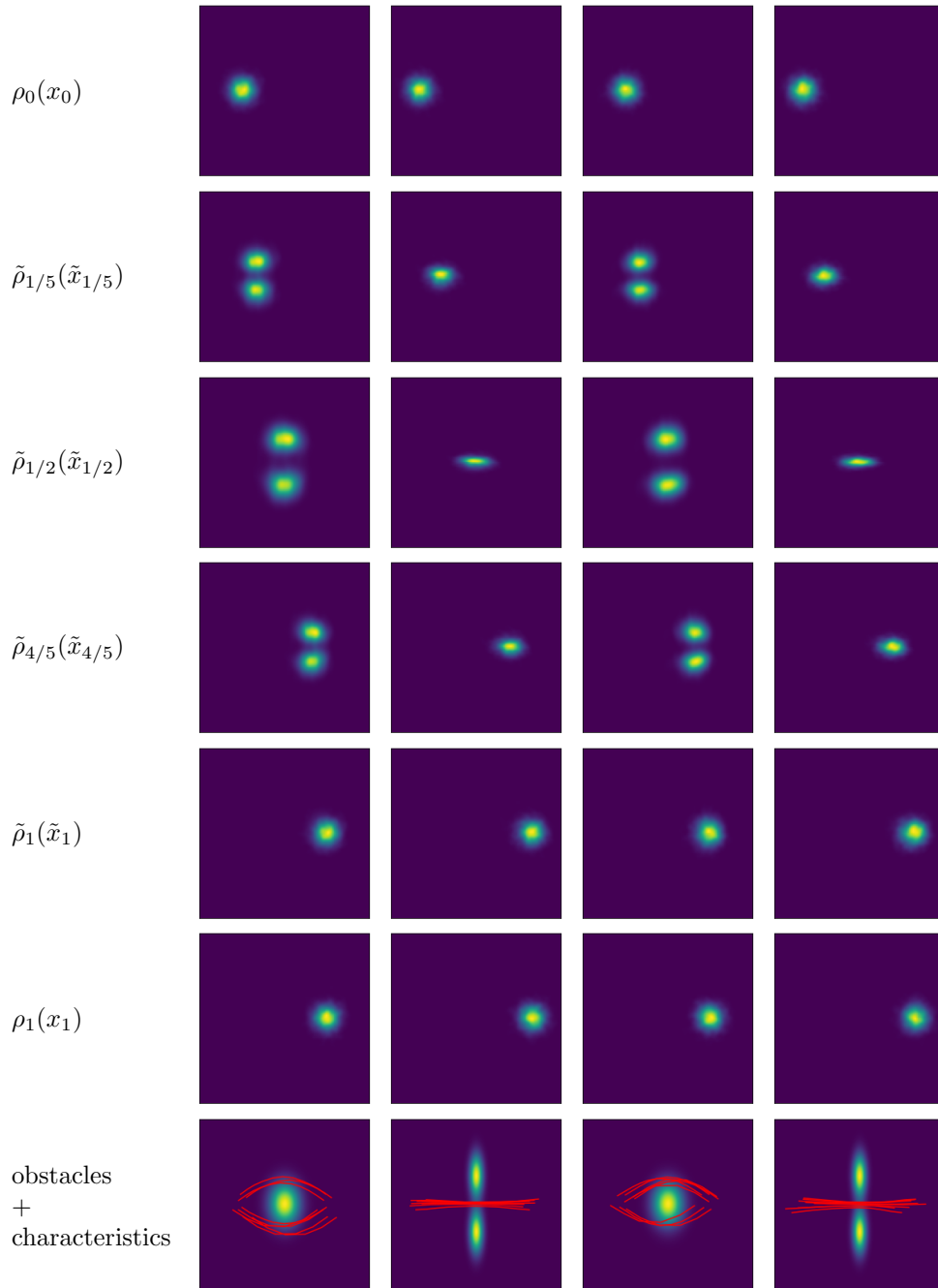


FIG. 3.4. Illustration of the crowd motion problem at $d = 2$ (left two columns) and $d = 5$ (right two columns).

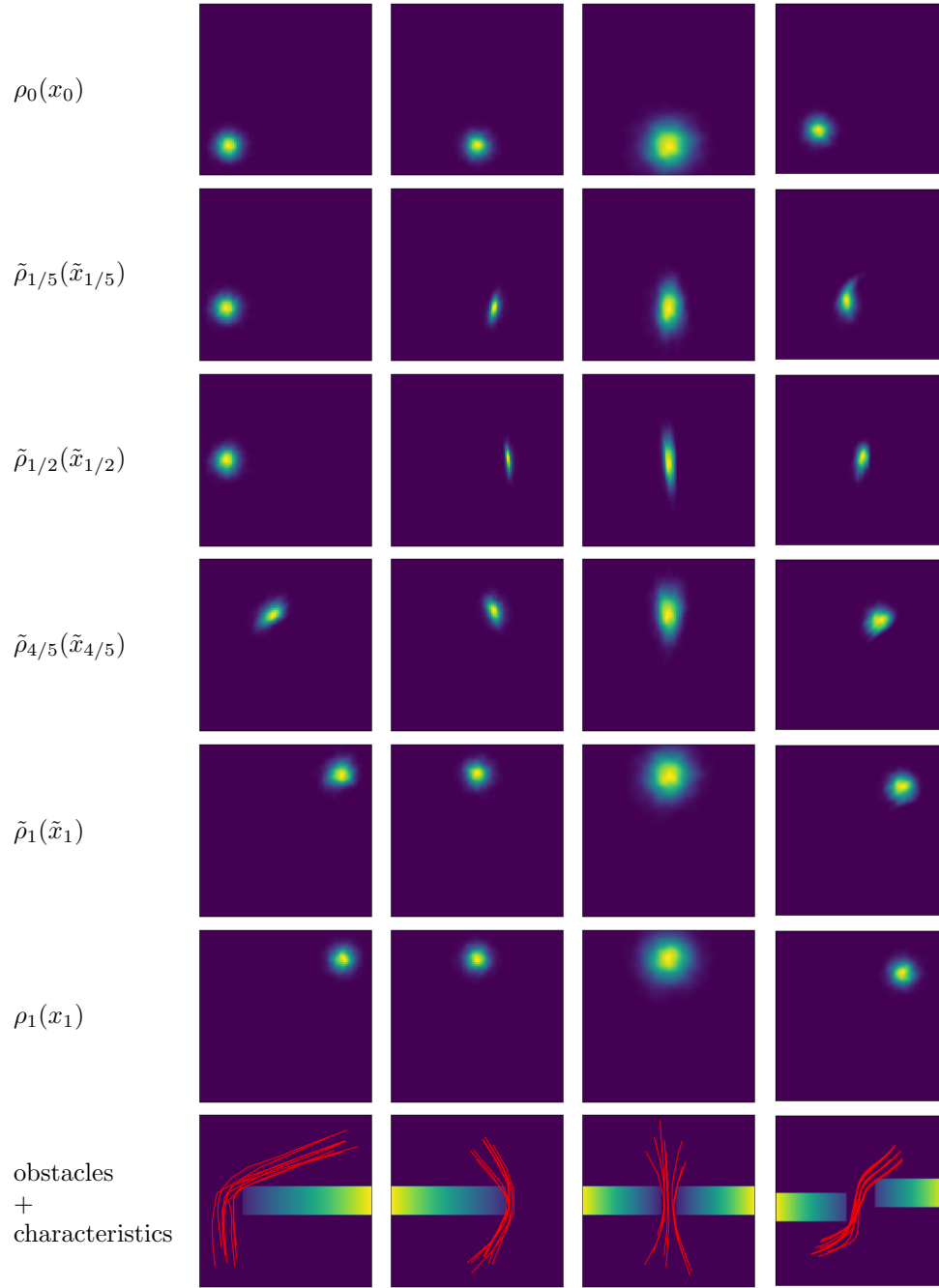


FIG. 3.5. Illustration of the crowd motion problem at $d = 2$ for maze examples.